Identification of limit cycles for piecewise nonlinear aeroelastic systems

D.P. Jones*, I. Roberts, A.L. Gaitonde

Department of Aerospace Engineering, University of Bristol, University Walk, Room 2.40 Queens Building, Bristol BS8 1TR, UK

Abstract

This paper describes two methods for the analysis of aeroelastic systems with complex piecewise nonlinear structural stiffness. These methods are tested and compared for low speed incompressible and transonic flows. The first technique employed in this paper uses a new application of the analytical solution of linear algebraic systems, the second technique utilises logarithmic and tanh functions to both represent discrete nonlinearities and to act as a switch between different nonlinear areas. The transonic aerodynamic models used are generated using an eigenvalue realisation algorithm (ERA) which produces reduced order models (ROMs) from the pulse responses of time linearised Euler simulations. It is shown that such aerodynamic models are well suited to use with continuation methods. Flutter boundaries and limit cycle oscillations can then be rapidly identified with good accuracy.
© 2007 Elsevier Ltd. All rights reserved.

Keywords: Aeroelasticity; Limit cycle oscillations; Continuation; Reduced order models

1. Introduction

The aim of this paper is to describe the development of efficient methods for the solution of structurally nonlinear aeroelastic systems. The requirement for efficient prediction has been driven by the military aircraft industry that is required to design for operation ever nearer the flight envelope of its aircraft. The requirement to generate realistic results rapidly throughout all regimes is restricted by two major factors. The first restriction is the representation of system nonlinearities which often requires the designer to perform multiple time integration runs as the system is often initial condition dependent (Price et al., 1994; Conner et al., 1996; Lee et al., 1999). The second restriction on aeroelastic prediction is the simulation of the transonic aerodynamics. The time required by transonic flow solvers to generate solutions for fully coupled systems is prohibitive, often requiring many hours or days to generate a single solution. When these two factors are combined, prediction via time-integration becomes impractical.

One technique to allow the practical analysis of transonic aeroelastic systems is the use of reduced order models (ROMs). These ROMs can be generated in many ways from the full dynamic transonic flow solvers that have a large number of degrees of freedom (dof). A method recently developed requires a limited number of linear pulse responses in the structural dof to be performed on the linearised Euler equations (Silva, 1997). In these linearised equations it is assumed that the flow structure remains unchanged through the motion (Kreiselmaier and Lschka, 2000), i.e., shock

---

*Corresponding author.

E-mail address: dorian.jones@bristol.ac.uk (D.P. Jones).

Nomenclature

A, B, C, D	aerodynamic (and general aeroelastic) state-space matrices	r_β	control surface radius of gyration about the hinge line
b	semichord	U	freestream air speed
$C_h\ \hat{C}_h\ \bar{C}_h$	total, unsteady perturbation and steady lift coefficient	U^*	nondimensional speed index
		U_L	air speed at flutter boundary of linear aeroelastic model
$C_\alpha\ \hat{C}_\alpha\ \bar{C}_\alpha$	total, unsteady perturbation and steady elastic axis moment coefficient	x_α	position of c.g aft of elastic axis
		x_β	position of c.g of flap aft of flap elastic axis
$C_\beta\ \hat{C}_\beta\ \bar{C}_\beta$	total, unsteady perturbation and steady hinge moment coefficients	$\mathbf{X}_A$	aerodynamic/augmented states
h	heave displacement	α	aerofoil angle of attack
$k_{h/\alpha/\beta}$	linear structural stiffness components	β	ratio of specific heats
m	aerofoil mass	ε	fit parameter for hyperbolic function approximation
M	restoring heave force on aerofoil	λ	continuation parameter
N/G	restoring moment on flap/aerofoil	ω_α	natural pitch frequency of aerofoil
r_α	aerofoil radius of gyration about the elastic axis	ω_β	natural pitch frequency of flap
		ω_h	natural heave frequency of aerofoil

waves and separations do not appear or disappear. It is possible to use the convolution of the pulse responses to recreate the overall responses of the aerodynamics. Such methods have been implemented but suffer in that they require long-time histories to be taken (Gaitonde and Jones, 2002). The method adopted in this paper uses the observation that the aeroelastic response is often dominated by relatively few modes of the system; therefore it is possible to use standard system identification techniques to create a state-space model of the system (Jones and Gaitonde, 2002). To achieve this objective, an eigenvalue realisation algorithm (ERA) (Juang and Pappa, 1985) is used to construct a ROM that is discrete in time. This discrete ROM is then transformed to generate a time-continuous ROM of the original continuous linearised Euler system (Gaitonde and Jones, 2003). As the ROM produced is in state-space form, it becomes possible to use aeroelastic analysis techniques that have previously been used for simplified low speed flows. A further point to note is that modal mass and stiffness can be modified without having to reconstruct the ROM.

The analysis of aeroelastic systems with nonlinear structures has often relied upon the performance of multiple time integration runs to capture the systems properties fully (Price et al., 1994; Conner et al., 1996; Lee et al., 1999). Such tasks are often impractically time consuming and inaccurate (Conner et al., 1996). A system that is frequently employed is the harmonic balance method, which uses an equivalent stiffness to represent the nonlinear stiffness present within the system (Luber, 1998; Dimitriadis and Cooper, 1999). This gives an approximate response but misses out many modes of the system that are created by the inclusion of discontinuities in discrete nonlinear structures. Lin and Cheng (1993) identified the importance of the accurate capture of the time, and system state, at which the system properties change (referred to as switching points) in a piecewise nonlinear system. They found that the resultant solutions were often different when the switching points were not captured to sufficient accuracy. Conner et al. (1996) solved this problem by using Henon's (1982) method to identify these switching points in a single step, as opposed to an iterative procedure, in a time stepping scheme. Henon's method can be applied to a general system with any form of discrete nonlinearity within the structure, but still requires multiple time-integration runs to be performed for a complete analysis of the aeroelastic system. Recently, the use of the centre-manifold theory to generate normal-form solutions for systems with continuous nonlinearities has also been developed (Liu et al., 2000; Sedaghat et al., 2000).

Several research centres have developed techniques for the analysis of systems with discrete nonlinearities. For such systems the capture of the boundary between linear areas is the most important factor as stated above. This motivated the work of Roberts et al. (2002) and Wong et al. (2001). Both methods use the nonlinear state as the independent variable and are therefore able to step directly from one switching point to the next. Such techniques generate accurate results but are time consuming, as the solver must ensure that switching points are not skipped (Roberts et al., 2002). This method, although a step forward from simple time integration, does not alleviate the problem of initial condition dependence, and multiple runs must be performed to identify all solutions.

The first technique described in this paper will extend this work to incorporate algebraic numerical continuation software. In this technique, all the possible solutions for a period-*n* solution are found from a single time integration run which is used as a starting point for the numerical continuation. With such a method in place the user is required to perform only as many time integration and continuation runs as there are bifurcation branches to be studied. Therefore,

the problem of initial condition dependence has been considerably reduced but not removed. Note that the branch reached by the time integration used to start the calculation is still dependant on the initial condition and if the number and nature of the branches is unknown beforehand then a series of time integrations may still be required to ensure all branches are found. The second method presented removes the need for any time integration and hence the initial condition dependence.

The second method described in this paper allows the aeroelastic system to be recast such that the numerical continuation of a set of ordinary differential equations may be used. Using a hyperbolic function approximation for the discrete nonlinearities satisfies the requirement of the software used in this work for a continuous set of equations (Doedel et al., 1998). Alighanbari and Price (1996) previously used rational approximations to simulate a discrete nonlinearity. However, the approximation was of relatively low order and therefore did not capture the nonlinearity exactly. Additionally, the method that was advocated by Alighanbari and Price requires a significant increase in polynomial order to increase simulation accuracy. A benefit of the second method presented here is that a single system variable controls the accuracy of the approximation. It will be shown that such a method has many advantages when applied to numerical continuation as this ''closeness of fit'' variable can be set as the continuation parameter.

The techniques presented in this paper are tested on the analysis of two two-dimensional (2-D) aeroelastic systems. The first system is incompressible and demonstrates the behaviour of the two methods when compared to previous analysis. The second is a transonic case where the results of the methods are compared to those obtained from time marching results using a full CFD Euler analysis to represent the aerodynamics.

2. Linear aeroelastic models

2.1. Incompressible two-degree-of-freedom model for 2-D aerofoil

The first system used in this work is a two-degree-of-freedom (2-dof) aerofoil system, with vertical heave translation and rotational pitch motion. It is assumed that there is no structural damping and the system has linear stiffness. The general equations of motions are

$$m\ddot{h}(t) + mx_\alpha b\ddot{\alpha}(t) + M(t) = P(t), \quad M(t) = k_h h(t),$$
$$mx_\alpha b\ddot{h}(t) + mr_\alpha^2 b^2 \ddot{\alpha}(t) + G(t) = R(t), \quad G(t) = k_\alpha \alpha(t), \tag{1}$$

where m is the aerofoil mass, $P(t)$ is the external force applied vertically, $R(t)$ is the moment applied about the elastic axis, $k_{h/\alpha}$ is the heave/pitch stiffness, and r_α is the radius of gyration about the elastic axis; the geometry is defined in Fig. 1.

The aerodynamic model used to provide the force and moment terms for this case is derived from Fung (1993), which is based on the unsteady aerodynamic forces acting on a thin aerofoil in a 2-D incompressible flow. The model is converted to ODE form for this test case using the method of Lee et al. (1997).

The formulation used for the coupled aeroelastic system is from Wong et al. (2001), where the nondimensionalisation of length, mass and time is by: semi-chord, relative air density and the semi-chord transit time, respectively. This gives the nondimensional time, $\bar{t}$, air mass ratio, μ, and speed index, U^*, values of

$$\bar{t} = \frac{U}{b}t, \quad \mu = \frac{m}{\pi\rho b^2}, \quad U^* = \frac{U}{b\omega_\alpha}, \tag{2}$$

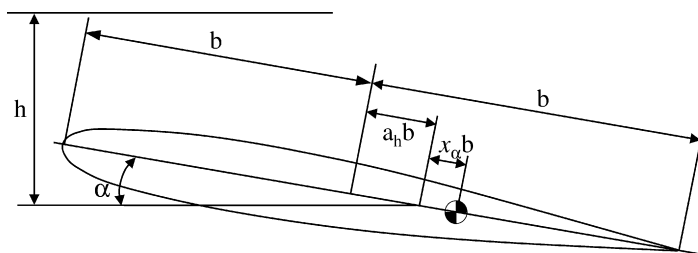where ω_α is the torsional (pitch) natural frequency of vibration.

Fig. 1. The two-degree-of-freedom aeroelastic system.

Defining the structural systems state variables as

$$\mathbf{U}_1 = \begin{bmatrix} h \\ \alpha \end{bmatrix}, \quad \mathbf{U}_2 = \begin{bmatrix} \dot{h} \\ \dot{\alpha} \end{bmatrix}, \tag{3}$$

the coupled linear system can be written in the form:

$$\begin{bmatrix} \dot{\mathbf{U}}_1 \\ \dot{\mathbf{U}}_2 \\ \dot{\mathbf{X}}_A \end{bmatrix} = [A] \begin{bmatrix} \mathbf{U}_1 \\ \mathbf{U}_2 \\ \mathbf{X}_A \end{bmatrix}, \tag{4}$$

where $\mathbf{X}_A$ is the vector of augmented states introduced by the aerodynamic model.

2.2. Compressible three-degree-of-freedom structural model for 2-D aerofoil

The second system used in this work is a three-degree-of-freedom (3-dof) aerofoil system, with vertical heave translation, rotational pitch and control surface pitch motion. Again it is assumed that there is no structural damping and the system has linear stiffness. The general equations of motions are therefore

$$m\ddot{h}(t) + mx_\alpha b\ddot{\alpha}(t) + mx_\beta b\ddot{\beta}(t) + M(t) = P(t), \quad M(t) = k_h h(t),$$
$$mx_\alpha b\ddot{h}(t) + mr_\alpha^2 b^2\ddot{\alpha}(t) + [(c_\beta - a_h)x_\beta + r_\beta^2]mb^2\ddot{\beta}(t) + G(t) = R(t), \quad G(t) = k_\alpha \alpha(t),$$
$$mx_\beta b\ddot{h}(t) + [(c_\beta - a_h)x_\beta + r_\beta^2]mb^2\ddot{\alpha}(t) + mr_\beta^2 b^2\ddot{\beta}(t) + N(t) = Q(t), \quad N(t) = k_\beta \beta(t), \tag{5}$$

where additional to the previous definitions for the 2-dof model, $Q(t)$ is the moment applied about the hinge, k_β is the rotational stiffness about the hinge, and r_β is the control surface radius of gyration about the hinge line; the geometry is defined in Fig. 2.

The length and mass are nondimensionalised as for the incompressible 2-dof model. However, the time is nondimensionalised in the same way as the aerodynamic models used in this work to give

$$\bar{t} = \frac{a_\infty}{b\sqrt{\gamma}}t, \quad U^* = \frac{U}{b\omega_\alpha\sqrt{\gamma}}. \tag{6}$$

For consistency with the incompressible model described in the previous section, the structural state variables are defined by the vectors $\mathbf{U}_1$ and $\mathbf{U}_2$:

$$\mathbf{U}_1 = \begin{bmatrix} h \\ \alpha \\ \beta \end{bmatrix}, \quad \mathbf{U}_2 = \begin{bmatrix} \dot{h} \\ \dot{\alpha} \\ \dot{\beta} \end{bmatrix}. \tag{7}$$

The aerodynamic inputs are defined in terms of the: lift, elastic axis moment and hinge moment coefficients. In the following sections these will be split into their mean components and perturbations:

$$\begin{bmatrix} C_l \\ C_m \\ C_h \end{bmatrix} = \begin{bmatrix} \hat{C}_l + \bar{C}_l \\ \hat{C}_m + \bar{C}_m \\ \hat{C}_h + \bar{C}_h \end{bmatrix}. \tag{8}$$
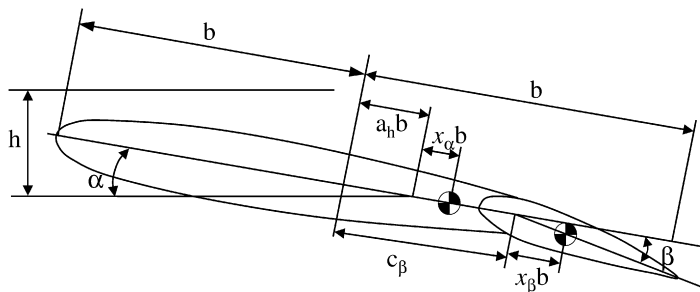

Fig. 2. The three-degree-of-freedom aeroelastic system.

This structural model is coupled with two aerodynamic models. The first is a nonlinear finite volume solution of the Euler equations. The second is a ROM based on the local linearisation of the same Euler CFD code about a full nonlinear mean solution. The full model was included in this work to check the behaviour of the ROM in modelling LCO's in the transonic region.

2.2.1. Finite volume Euler aerodynamic model

The compressible aerodynamic code used in this work is a cell centred finite volume Euler method with artificial dissipation (Jameson et al., 1981). For unsteady flows on moving meshes this Euler solver uses a dual time stepping scheme with a second-order implicit real time step and a modified four-stage Runge–Kutta scheme (Melson et al., 1993), is used in pseudo-time. A detailed account of the implementation is given by Gaitonde (1994).

A strong coupling of the full Euler code with the structural equations uses the scheme developed by Newmark (Bathe, 1982) and involves a direct integration of the surface pressures. The method has been applied to the same system by Djayapertapa (2001). A difficulty of applying the Newmark scheme to nonlinear structural problems such as cubic stiffening and freeplay, is that the solution must be locally linearised at each time step. This results in the average of the stiffness over the time step being used and there may be some loss of accuracy in the solution at switching points in the structural behaviour.

2.2.2. Three-degree-of-freedom aerodynamic ROM

A brief description of the method used to obtain the ROM of the Euler equations is given here though a more detailed discussion can be found in Gaitonde and Jones (2002, 2003). The time-linearised Euler equations, which are produced from a local linearisation of the full Euler equations about a mean base flow, could be written in state-space form as

$$\dot{\mathbf{X}}_A = A\mathbf{X}_A + B\mathbf{U}, \quad \mathbf{Y} = C\mathbf{X}_A + D\mathbf{U}, \tag{9}$$

where A, B, C and D are system matrices. The vectors $\mathbf{U}$ and $\mathbf{X}_A$ are

$$\mathbf{U} = \begin{bmatrix} h & \alpha & \beta & \dot{h} & \dot{\alpha} & \dot{\beta} \end{bmatrix}^{\mathrm{T}}, \quad \mathbf{X}_A = \begin{bmatrix} \hat{\rho}_1 & \hat{u}_1 & \hat{v}_1 & \hat{p}_1 & \cdots & \hat{\rho}_N & \hat{u}_N & \hat{v}_N & \hat{p}_N \end{bmatrix}^{\mathrm{T}}. \tag{10}$$

The terms in the $\mathbf{X}_A$ vector are the perturbations from the nonlinear mean in the density speed and pressure at all the N cells in the finite volume computational domain. The vector $\mathbf{Y}$ is the output, which can be any quantity that can be calculated from the available data. For the aeroelastic system described previously the required output is

$$\mathbf{Y} = \begin{bmatrix} \hat{C}_l \\ \hat{C}_m \\ \hat{C}_h \end{bmatrix}. \tag{11}$$

The CFD code used to solve the linearised Euler equations is discretised in time using a first-order implicit approximation to the time derivative. This discrete system can be written as

$$\tilde{\mathbf{X}}_k = \tilde{A}\tilde{\mathbf{X}}_{k-1} + \tilde{B}\tilde{\mathbf{U}}_k, \quad \tilde{\mathbf{Y}}_k = C\tilde{\mathbf{X}}_k + D\tilde{\mathbf{U}}_k, \tag{12}$$

where the discrete approximations to $\mathbf{X}$, $\mathbf{U}$ and $\mathbf{Y}$ are denoted by a tilde, k is the index of the time step Δt and the relationship between the discrete and continuous system matrices is given by

$$\tilde{A} = (I - A\Delta t)^{-1}, \quad \tilde{B} = (I - A\Delta t)^{-1}B\Delta t, \quad \tilde{C} = C, \quad \tilde{D} = D. \tag{13}$$

By applying impulses to each of the inputs of the vector $\mathbf{U}$, the discrete impulse responses are formed in the output variable $\tilde{\mathbf{Y}}_k$. These outputs are used to construct the discrete time Hankel matrix and an ERA algorithm (Juang and Pappa, 1985; Jones and Gaitonde, 2002) is then used to identify the discrete system matrices from these impulse responses. The continuous system matrices can then be approximated using the inverse of the first-order implicit time discretisation, i.e.

$$A_{\mathrm{ROM}} = \frac{(I - \tilde{A}_{\mathrm{ERA}}^{-1})}{\Delta t}, \quad B_{\mathrm{ROM}} = \frac{(I - A_{\mathrm{ROM}}\Delta t)\tilde{B}_{\mathrm{ERA}}}{\Delta t}, \quad C_{\mathrm{ROM}} = \tilde{C}_{\mathrm{ERA}}, \quad D_{\mathrm{ROM}} = \tilde{D}_{\mathrm{ERA}}. \tag{14}$$

2.2.3. Structural coupling model for 2-D aerofoil

Combining the representation of the structural motion equations with the aerodynamic state-space equation the aeroelastic model of the system is obtained as

$$
\begin{bmatrix} \dot{\mathbf{U}}_1 \\ \dot{\mathbf{U}}_2 \\ \dot{\mathbf{X}}_A \end{bmatrix} = [A] \begin{bmatrix} \mathbf{U}_1 \\ \mathbf{U}_2 \\ \mathbf{X}_A \end{bmatrix} + \begin{bmatrix} \mathbf{0} \\ \bar{\mathbf{C}} \\ \mathbf{0} \end{bmatrix},
\tag{15}
$$

where

$$
\bar{\mathbf{C}} = [F] \begin{bmatrix} \bar{C}_l \\ \bar{C}_m \\ \bar{C}_h \end{bmatrix},
\tag{16}
$$

and $[F]$ represents an aerodynamic transformation matrix. With the aeroelastic state equations in this form it is now possible to utilise the same analysis techniques for the transonic test cases as will be used for the low speed analysis.

Thus far we have considered linear structural models. In the following section the inclusion of nonlinear stiffness terms is considered.

3. Analysis of piecewise nonlinear aeroelastic systems

In Eqs. (1) and (5) the stiffness terms are represented by the terms M, G and N. The introduction of nonlinear stiffness requires these linear relations to be replaced. The result is that these stiffness terms will form an additional nonlinear vector in the coupled aeroelastic state-space systems, so that Eqs. (4) and (15) become

$$
\begin{bmatrix} \dot{\mathbf{U}}_1 \\ \dot{\mathbf{U}}_2 \\ \dot{\mathbf{X}}_A \end{bmatrix} = [A] \begin{bmatrix} \mathbf{U}_1 \\ \mathbf{U}_2 \\ \mathbf{X}_A \end{bmatrix} + \begin{bmatrix} \mathbf{0} \\ \mathbf{b} \\ \mathbf{0} \end{bmatrix},
\tag{17}
$$

where $\mathbf{b}$ contains the nonlinear component.

3.1. Boundary identification and algebraic continuation

If the nonlinear system is made up of purely piecewise linear components, then we can calculate the solution of a linear system in each region separately and then combine these solutions. The resulting system can be solved using what will be described in this work as algebraic continuation. We shall first start by recapping the solution of a linear state-space system.

A general linear state-space system of order n is given by

$$
\dot{\mathbf{x}} = [A]\mathbf{x} + \mathbf{b}_0.
\tag{18}
$$

The general solution of this linear state-space system is given by

$$
\mathbf{x}(t) = e^{[A]t}(\mathbf{x}(0) + [A]^{-1}\mathbf{b}_0) - [A]^{-1}\mathbf{b}_0,
\tag{19}
$$

where $\mathbf{x}(0)$ is the set of initial conditions. This is equivalent to the solution of a piecewise linear system where the solution remains in a single linear region having entered that region at time zero. If piecewise nonlinear systems are to be analysed, the times at which the solution crosses from one linear region to another must be found. Therefore, we now solve this system for the time at which the solution exits the linear region.

If the solution exits this linear region when the value of the ith state reaches x_i, then the time t at which the system crosses this boundary is defined by

$$
x_i = \mathbf{e}_i \{ e^{[A]t}(\mathbf{x}(0) + [A]^{-1}\mathbf{b}_0) - [A]^{-1}\mathbf{b}_0 \},
\tag{20}
$$

where the unit vector $\mathbf{e}_i$ isolates the ith dof and is constructed by placing a one in the ith component and zero in all others. Eq. (20) has no general analytical solution for t, instead numerical root finding would be required to find the first valid solution. The direct solution of this equation will not be considered further, as the algebraic continuation method described below does not require it. However, Eq. (20) is required to define the solution path after we first consider the continuation software used in this work.

An algebraic solution sequence can be used within the continuation software AUTO (Doedel et al., 1998), this solves systems of the form:

$$f(\mathbf{x}, \lambda) = \mathbf{0}, \quad f(\mathbf{x}, \lambda), \mathbf{x} \in R^n, \tag{21}$$

where λ is the continuation parameter, which can be any nonstate variable that is used within the system of equations, e.g., aeroelastic systems could use the air speed or a particular stiffness as the continuation parameter. This general description does not exclude LCO solutions as the states $\mathbf{x}$ can include augmented states that represent the period of oscillation and LCO phase relationships. Given the previous analysis for the solution of a state-space system in a linear region, it is a relatively straightforward process to recast the equations governing the periodic solution of a piecewise linear system in the above form (Eq. (21)). This will be made clearer by the simple example below.

Consider a nonlinear system, written in the form of Eq. (17), comprising of three linear regions: 1, 2, 3 each defined by state matrices $[A] = [A_1], [A_2], [A_3]$ and vectors $\mathbf{b} = \mathbf{b}_1, \mathbf{b}_2, \mathbf{b}_3$, respectively. A simple example of such a system is shown in Fig. 3 for a freeplay in stiffness, where region 2 represents the central, zero-stiffness, region. The boundary between the regions $1 \leftrightarrow 2$ and $2 \leftrightarrow 3$ is fixed by values of the ith state of x_i^{1-2} and x_i^{2-3}, respectively. In the case of the freeplay in stiffness shown in Fig. 3, the values of x_i^{1-2} and x_i^{2-3} represent the values of displacement which form the upper and lower bounds to the freeplay region. A period-one limit cycle moving in the orbit $2 \rightarrow 3 \rightarrow 2 \rightarrow 1$ is defined by the four equations for times at which the solution crosses the region boundaries:

$$\begin{aligned}
\mathbf{e}_i\{e^{[A_2]t_1}(\mathbf{x}(0) + [A_2]^{-1}\mathbf{b}_2) - [A_2]^{-1}\mathbf{b}_2\} - x_i^{2-3} &= 0, \\
\mathbf{e}_i\{e^{[A_3]t_2}(\mathbf{x}(t_1) + [A_3]^{-1}\mathbf{b}_3) - [A_3]^{-1}\mathbf{b}_3\} - x_i^{2-3} &= 0, \\
\mathbf{e}_i\{e^{[A_2]t_3}(\mathbf{x}(t_2) + [A_2]^{-1}\mathbf{b}_2) - [A_2]^{-1}\mathbf{b}_2\} - x_i^{1-2} &= 0, \\
\mathbf{e}_i\{e^{[A_1]t_4}(\mathbf{x}(t_3) + [A_1]^{-1}\mathbf{b}_1) - [A_1]^{-1}\mathbf{b}_1\} - x_i^{1-2} &= 0,
\end{aligned} \tag{22}$$

and a periodicity relationship given by the n equations

$$\mathbf{x}(0) + \mathbf{x}(t_4) = \mathbf{0}. \tag{23}$$

Eqs. (22) and (23) are then combined to form a system, as in Eq. (21), which is solved using algebraic continuation.

The generalisation of the equations required for a limit cycle with a larger period or harmonics would be too unwieldy. However, it can be seen from Eqs. (22) and (23) that a period m limit cycle would require $4m+n$ equations. It should also be noted that for practical implementation further equations are required to identify important data such as the maxima of the structural states in each LCO and region.

The major difficulty of this method is that the trajectory of the LCO solution must be known *a priori*, therefore an initial solution may be required from some other method for each branch of the bifurcation diagram. However, once a single solution is found then the algebraic continuation method can be used to identify all other LCO solutions along
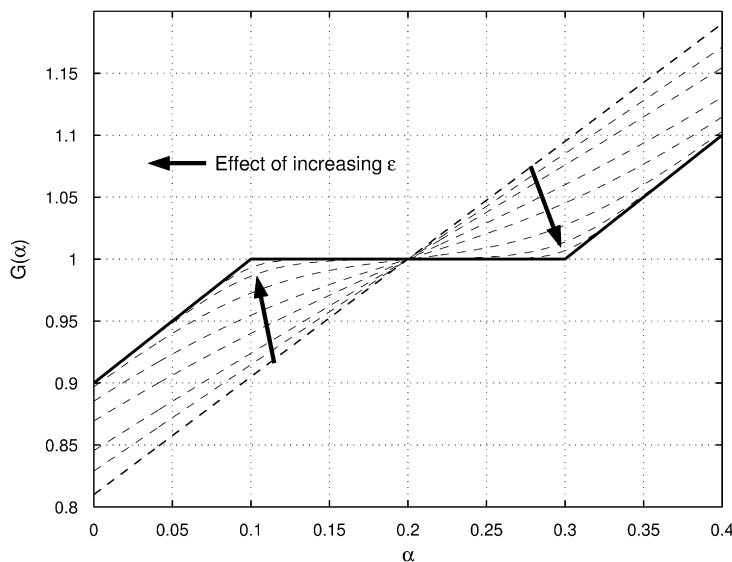

Fig. 3. Logarithmic approximations to freeplay, dashed lines show varying values of fit parameter ε (values from 0 to 10,000).

that branch of the bifurcation diagram. A further current limitation of this method is that the algebraic continuation method does not allow the stability to be assessed, as there is no explicit Jacobian matrix evaluation. However, the stability of the branches can usually be inferred by assuming a change in stability at the branch and fold points of the bifurcation diagram; see for instance Roberts (2004).

3.2. Hyperbolic approximation of nonlinear stiffness terms and numerical continuation

In this section, the use of combinations of tanh and logarithmic functions to represent piecewise nonlinear structures is explained. Numerical continuation software which will be used to analyse the coupled systems requires that the set of ordinary differential equations are continuously differential in the range studied. As systems with discrete nonlinearities are not continuously differentiable at the switching points a smooth function may be employed to approximate the discrete function to various levels of accuracy. In the discussion below it is shown that logarithmic and tanh functions can be utilised in the description of some common nonlinearities that have been studied in this work.

3.2.1. Some examples of continuous approximations to piecewise nonlinear systems

Freeplay is a discontinuity that is often studied in aeroelasticity, as it is a common occurrence within the actuated dof of systems (Luber, 1998). Fig. 3 shows a typical restoring moment/control surface rotation graph for such a nonlinearity. The representation of a freeplay with a single function has been attempted previously by Alighanbari and Price (1996). In their studies a rational function approximation to the freeplay was used which proved to be lacking in some areas. In their results, Alighanbari and Price (1996) showed limit cycle oscillation occurring solely within the central freeplay region. This is not possible because, in theory, the system of equations for this region is completely linear. A far more suitable approximation can be obtained using logarithmic functions.

It has been found that a freeplay can be represented by

$$G(\alpha) = \frac{1}{\varepsilon} \ln \frac{1 + e^{\varepsilon(\alpha - \alpha_u)}}{1 + e^{-\varepsilon(\alpha - \alpha_l)}} + G_0, \tag{24}$$

where G_0 is the vertical offset, to represent preload upon the system, while α_u and α_l are the upper and lower boundaries of the freeplay region. ε is a scaling factor that determines the accuracy of the approximation. As ε tends to infinity the approximation approaches the actual freeplay. This is also shown in Fig. 3 for varying values of the fit parameter ε.

Hysteresis nonlinearities are observed in many dynamic systems and arise when friction couples with other nonlinearities such as freeplay. Representing a hysteresis curve, as shown in Fig. 4, by hyperbolic functions is an important application as it allows a system that is inherently nonlinear to be smoothly represented. When hysteresis is present within a system, two different paths are followed depending on whether the velocity of the particular dof is
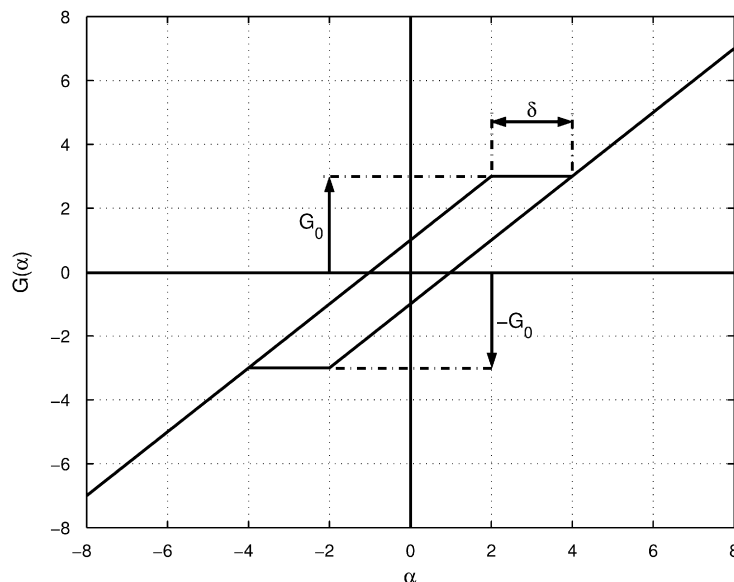

Fig. 4. Hysteresis nonlinearity.

positive or negative. When approximating hysteresis nonlinearity the authors noted that, in this form of hysteresis, the nonlinearity is essentially two offset freeplays. Therefore, using the tanh to form a Heavyside function it becomes possible to switch between the two freeplays using the boundary between positive and negative motion rate as the heavyside boundary. This allows a hysteresis in pitch to be approximated by

$$G(\alpha) = \frac{1}{2}(1 - \tanh(\varepsilon\dot{\alpha}))\left(\frac{1}{\varepsilon}\ln\frac{1 + e^{\varepsilon(\alpha-\alpha_{u+})}}{1 + e^{-\varepsilon(\alpha-\alpha_{l+})}} + G_+\right) + \frac{1}{2}(1 + \tanh(\varepsilon\dot{\alpha}))\left(\frac{1}{\varepsilon}\ln\frac{1 + e^{\varepsilon(\alpha-\alpha_{u-})}}{1 + e^{-\varepsilon(\alpha-\alpha_{l-})}} + G_-\right). \tag{25}$$

where α_u and α_l represent the upper and lower boundaries of the freeplay and the subscripts $+$ and $-$ denote the curves for positive and negative velocity, respectively. G_+ and G_- are the magnitudes of the system preloads that offset the curves from the $G(\alpha) = 0$ axis (Fig. 4 shows $G_+ = -G_- = G_0$). For this particular case it is noted that the representations of oscillations that occur solely within the loop of the hysteresis curve may not be accurately represented. This is because assumptions about the behaviour of the system within this low amplitude range are usually defined by a simple linear slope going through the origin of the axes.

Using these tools it can be seen that it is possible to represent a large range of nonlinearities and further to represent combinations of nonlinearities. Consider that the linear regions of each of the nonlinearities could be replaced by polynomial regions without any difficulty. Solutions of systems of this type will not be considered here but can be found in Roberts (2004). Once continuous approximations of any nonlinear systems have been made, numerical continuation can be used. How numerical continuation can be used will be discussed in the next section. Numerical continuation is not to be confused with the related algebraic continuation previously described, though both are implemented in the AUTO software.

3.2.2. Hyperbolic approximation of nonlinear stiffness terms and numerical continuation

Numerical continuation methods, such as those implemented in the software AUTO (Doedel et al., 1998), solve general order n ODE systems of the form:

$$\dot{\mathbf{x}} = f(\mathbf{x}(t), \lambda) = \mathbf{0}, \quad f(\mathbf{x}, \lambda), \mathbf{x} \in R^n, \tag{26}$$

where λ is again the continuation parameter that can be any nonstate variable that is used within the system of equations; e.g., aeroelastic systems could use the air speed or a particular stiffness as the continuation parameter. As for algebraic continuation this general description does not exclude LCO solutions as the states $\mathbf{x}$ can include augmented states that represent the period of oscillation and LCO phase relationships. These are described in many good textbooks (Seydel, 1994; Kuznetsov, 1995).

The hyperbolic functions used for approximating nonlinear terms are extremely useful tools when combined with numerical continuation software. When implementing nonlinearities within numerical continuation software, solvers find problems where solutions jump from convergent solutions to oscillatory solutions with reasonable amplitudes. A similar problem can be found at the end of bifurcation branches where the nature of the stable LCO can also jump significantly. For a smooth system the amplitudes of the oscillations tend to gradually increase from zero, whereas discrete functions suddenly have large amplitudes of oscillation as shown by Wong et al. (2001). The use of the hyperbolic approximations can circumvent these problems. If hyperbolic approximations are used, the "closeness-of-fit" variable ε can be set to the continuation parameter and gradually increased so the hyperbolic approximation approaches the discrete nonlinearity. Therefore, the system will not see any sudden jumps in amplitude for low values of ε. Once on a branch with an accurate approximation of the discrete nonlinearity, the required continuation parameter can be used for a fixed value of ε. The results for low values of ε used to reach the branch can then be ignored, as they do not represent the discrete behaviour accurately. The same technique can be used to bracket regions of chaotic behaviour, where the discretisation used in AUTO will break down.

4. Results

4.1. Incompressible 2-dof system

The accuracy and benefits of using the algebraic continuation and hyperbolic approximation methods are established by analysing the 2-dof aeroelastic model, described in Section 2.1 and Fig. 1, with the aerofoil parameters

$$a_h = -0.5, \quad x_\alpha = 0.25, \quad r_\alpha = 0.5, \quad \omega_\alpha = 0.2, \quad \mu = 100.0,$$

and discrete nonlinearities in the pitch dof.

Details of the case can be found in Wong et al. (2001). A freeplay nonlinearity, as shown in Fig. 3, is applied to the pitch dof only. This nonlinearity is defined by

$$G(\alpha) = \begin{cases} \alpha - 0.25° & \text{for} & \alpha < 0.25°, \\ 0 & \text{for} & 0.25° \leqslant \alpha \leqslant 0.75°, \\ \alpha - 0.75° & \text{for} & \alpha > 0.75°. \end{cases} \tag{27}$$

Comparison of the bifurcation diagrams of Wong et al. (2001) and the algebraic continuation method are shown for pitch and period in Figs. 5 and 6, respectively. Good agreement is achieved between the two techniques, as would be expected, as they are based on similar theory. However, the algebraic continuation method requires fewer analysis
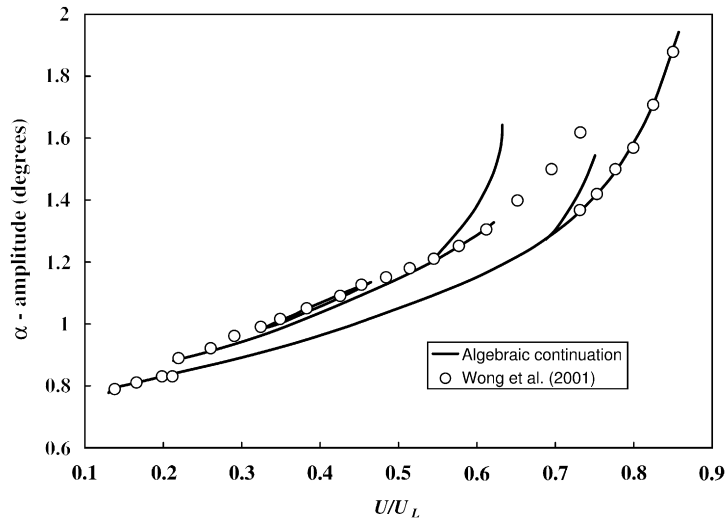
Fig. 5. 2-dof incompressible aeroelastic system, maximum pitch amplitude against ratio of flight speed to linear flutter velocity (U_L). Current results using algebraic continuation (stable and unstable branches) compared to results of Wong et al. (2001), stable branches only.
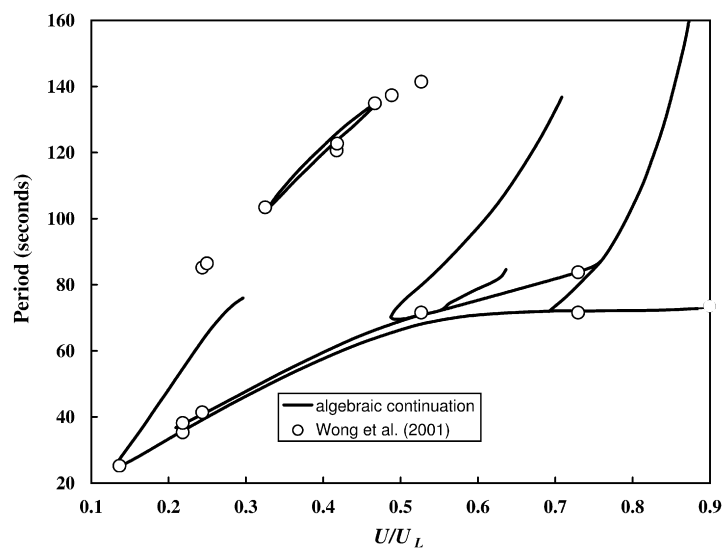

Fig. 6. 2-dof incompressible aeroelastic system. LCO period against ratio of flight speed to linear flutter velocity (U_L). Algebraic continuation (stable and unstable branches) compared with results of Wong et al. (2001), stable branches only.

stages and both stable and unstable branches are identified. Furthermore, systems with multiple stable branches are very difficult to explore unless a technique such as continuation is used.

Generally all branches of the algebraic continuation solutions that do not coincide with the results of Wong et al. are unstable. The discrepancy between the two techniques can be seen in the highest branch of the period bifurcation diagram. Wong et al. predict this stable period-2 harmonic branch continuing well above a value of U/U_L of 5, while algebraic continuation does not find this stable branch. A time marching technique (Roberts, 2004) very similar to that used by Wong et al. was used to investigate this region but no stable branch was found. The difference may be due to the sensitivity of the solution to the detailed implementation of the aeroelastic model.

Comparison of the bifurcation diagrams of Wong et al. (2001) and those produced using hyperbolic approximation with continuation analysis are shown for pitch and period in Figs. 7 and 8, respectively. Good agreement between the two techniques is achieved again. Regions of chaotic solutions exist around values of $U/U_L = 0.3$ and below $U/U_L = 0.5$ (Roberts, 2004). A rapid period doubling identified the onset of these chaotic regions which were then avoided by using ε as the continuation parameter. A stable period-2-harmonic solution exists between these two regions and had previously been identified by the algebraic continuation technique. However, the implementation of numerical
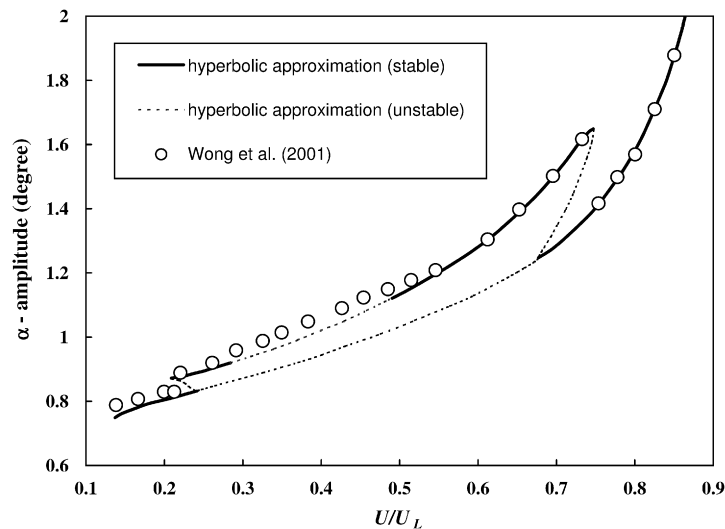

Fig. 7. 2-dof incompressible aeroelastic system, maximum pitch amplitude against ratio of flight speed to linear flutter velocity (U_L). Hyperbolic approximation (stable and unstable). Compared to results of Wong et al. (2001).
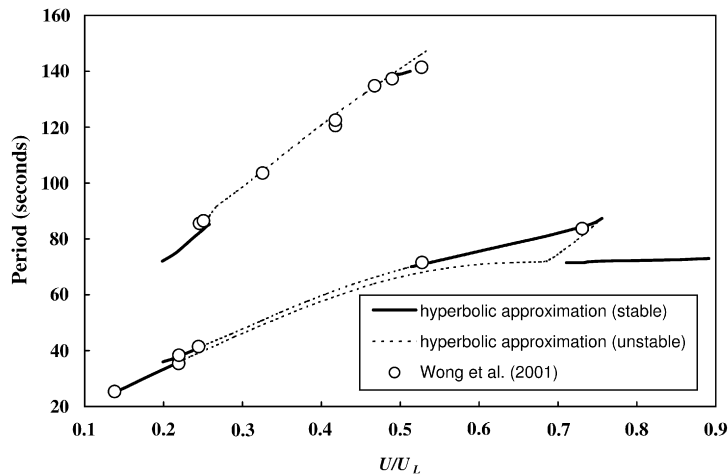

Fig. 8. 2-dof incompressible aeroelastic system. LCO period against ratio of flight speed to linear flutter velocity (U_L). Hyperbolic approximation (stable and unstable) compared to results of Wong et al. (2001).

continuation in AUTO initially identified this branch as unstable. This is due to the existence of two stable and symmetrical solutions, as shown in Fig. 9. The identification of stability uses initial condition perturbation (Doedel et al., 1998; Roberts, 2004), which mistakenly takes the branches to be unstable. Although the problem is resolved by increasing the accuracy of the analysis and only occurs due to the symmetry of the flow conditions, the example serves to highlight the difficulty such systems can present even for the current methods. Figs. 7 and 8 highlight this by showing the initial results with this stable branch identified as unstable by the continuation method.

4.2. Compressible 3-dof system

The results to be presented are intended to assess the accuracy of the continuation methods combined with the transonic ROM. These results are compared to time marching simulation solutions of the full Euler equations coupled with the nonlinear structural models. The test case uses a NACA64A010 aerofoil section and the linear model is the
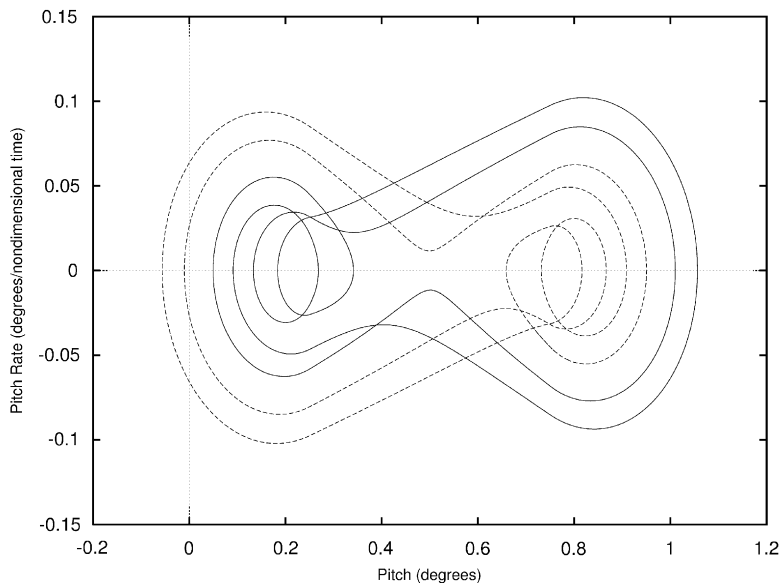

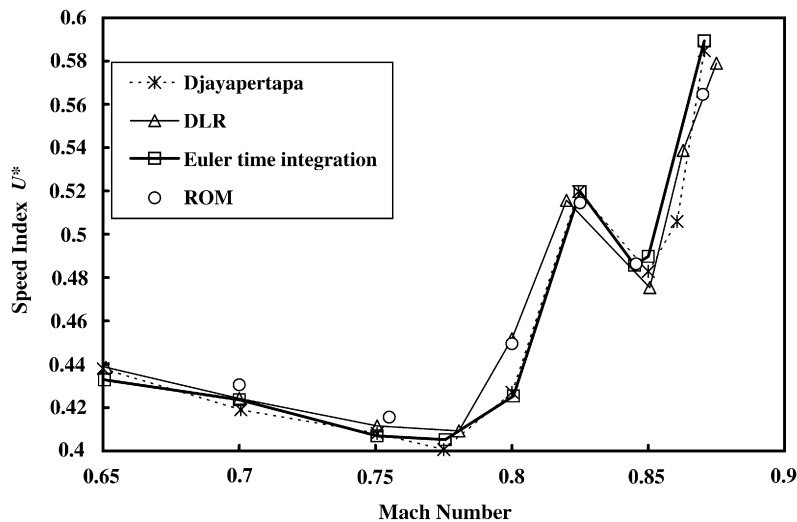Fig. 9. Phase projection of symmetric stable LCOs.

Fig. 10. Flutter boundary for transonic three-degree-of-freedom system.

same as used by Roberts (2004) and Djayapertapa, (2001). The 3-dof model parameters are

$$a_h = -0.2, \quad x_\alpha = 0.2, \quad r_\alpha = 0.5, \quad \omega_h/\omega_\alpha = 0.3, \quad \mu = 23.48,$$
$$x_\beta = 0.008, \quad r_\beta = 0.06, \quad \omega_\beta/\omega_\alpha = 1.5, \quad c_\beta = 0.5.$$

Initially the structural model used just the linear parameters; however, this was then modified to introduce a piecewise linear freeplay and hysteresis into the torsional stiffness of the flap. Both of these nonlinear cases were analysed using the hyperbolic function approximation and the algebraic continuation method.

The aerodynamic ROMs used in all the compressible analysis were the same size. Each ROM was of order 14 and constructed from pulse responses of 40 time steps for each Mach number.
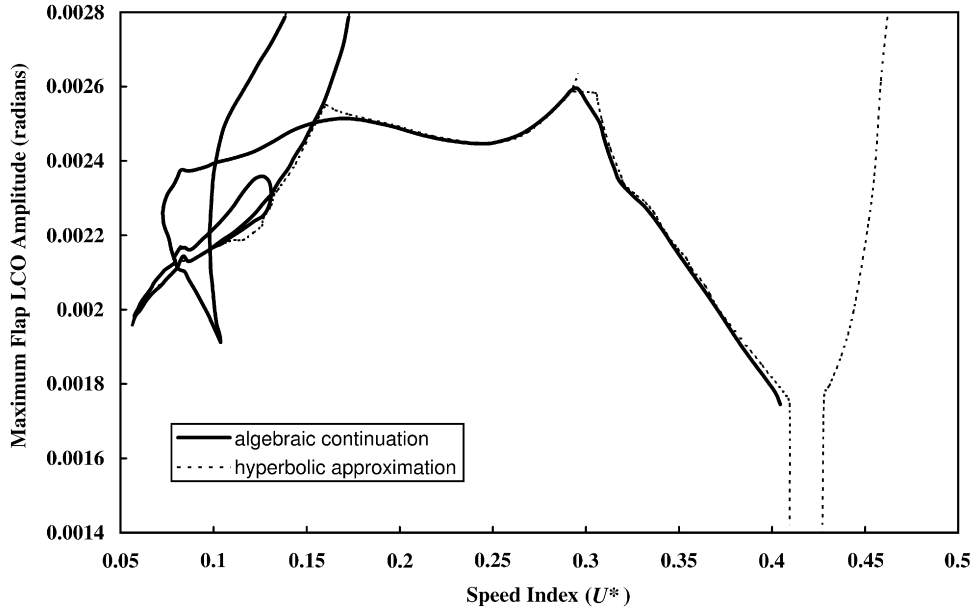

Fig. 11. Comparison of the bifurcation diagrams generated by algebraic continuation and hyperbolic approximation for a freeplaying system at Mach 0.845 (all branches initially identified as stable).
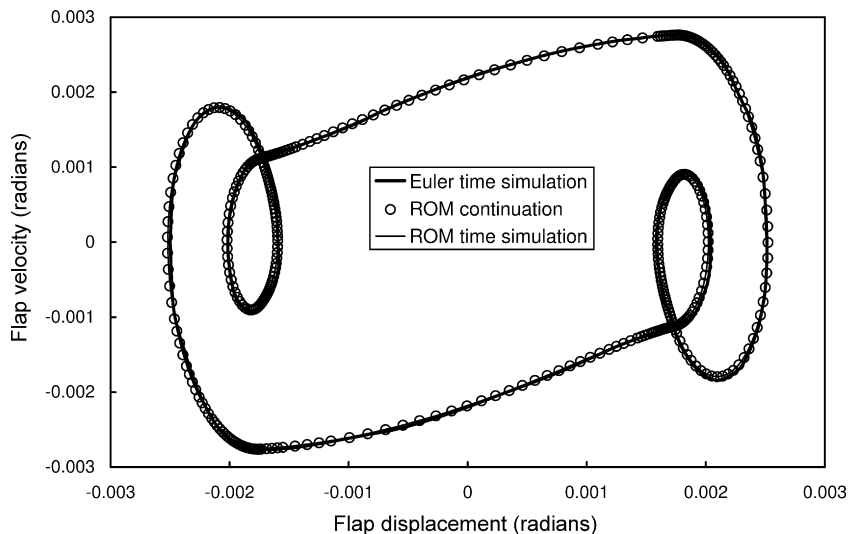

Fig. 12. Phase plane plot for a flap with freeplay nonlinearity at Mach 0.845 and $U^* = 0.176$.

4.2.1. Linear results

The flutter boundary for the linear stiffness case is shown in Fig. 10. The results are compared with the full Euler solution as well as the results of Djayapertapa (2001) and Schulze (1998). The results show good correlation between all solutions.

Even after the computational cost of the ROM construction is considered, the ROM flutter boundary calculation is at least two-orders of magnitude more efficient than the time stepping results using the full Euler equations. The results outlined in the following sections consider the introduction of a nonlinear structural model. Because of the initial condition dependence of any time stepping solution and the size of the original Euler system these results are inconceivable without the use of ROM aerodynamics.

4.2.2. Freeplay and hysteresis

The same structural model was then modified to demonstrate the power of the methods in approximating freeplay and hysteresis nonlinearities. The first case studied was a freeplay of $0.1°$ about a mean flap incidence of $0°$. Although this is a very small freeplay, it is consistent with the tolerance allowed for current aircraft maintenance schedules (US Department of Defense, 1993). The maximum flap LCO amplitude results for the freeplay nonlinearity at a Mach number of 0.845 are shown in Fig. 11. Note that as the flap amplitude falls below $0.1°$ (1.75×10^{-3} rad) there is no LCO as the motion would be contained entirely within the linear freeplay region. Comparison of the algebraic continuation and hyperbolic approximation techniques shows good agreement though the algebraic continuation seems to produce more complex behaviour at low values of the speed index. In reality these are a number of unstable branches incorrectly identified as stable by the inferred stability technique outlined by Roberts (2004). The difficulties of inferring the stability are a considerable drawback on the application of the current implementation of the algebraic continuation technique.

Differences between the two techniques are concentrated around branch points in the bifurcation diagram, i.e., positions where the nature of the LCO changes. An example of this is seen in Fig. 11 at a speed index of around 0.3. Conner et al. (1996) noted that incorrect identification of switching points resulted in incorrect solutions being achieved. From other analysis performed in the course of this work (Roberts, 2004), the nature of this inaccuracy has become more specified. The rigid speeds over which a particular LCO are found is smoothed, so that far away from the LCO onset even a coarse approximation to the boundary identification problem produces good results. Accordingly the highly accurate hyperbolic approximation to the nonlinear stiffness produces results very close to the algebraic continuation even at the branch points in the bifurcation diagram.

Comparisons of the ROM result with the full Euler solution are shown for individual points on the bifurcation diagram in Figs. 12–14. These figures show the phase plane plots for particular LCOs when calculated using an
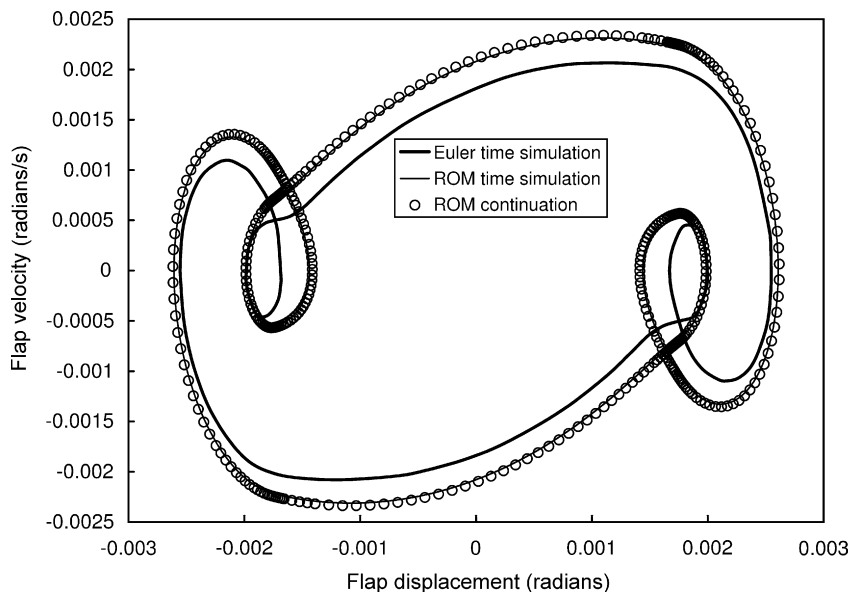

Fig. 13. Phase plane plot for a flap with freeplay nonlinearity at Mach 0.845 and $U^* = 0.295$.
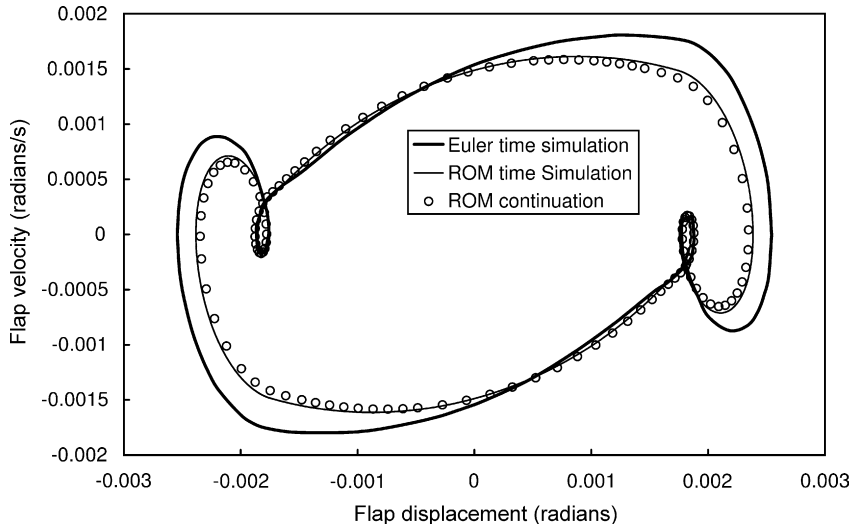
Fig. 14. Phase plane plot for a flap with freeplay nonlinearity at Mach 0.845 and $U^* = 0.320$.

implicit second-order time marching scheme applied to the full Euler equations and the ROM aerodynamic model. Both time marching cases are coupled with the nonlinear structural equations using the same Newmark scheme (Bathe, 1982), as mentioned in Section 2.2.1. These figures also show the results from the algebraic continuation. In all these figures the difference between the ROM solution using algebraic continuation and time simulation is small. This suggests that the error due to the accurate capturing of switching points is small for the time simulations considered.

The three Figs. 12–14 show the general trend that, for a fixed order of aerodynamic ROM, the accuracy of the coupled system decreases as the speed index increases. Most importantly, however, it must be noted that in our experience the structure of the periodic orbit is preserved. A great deal of work is still required to quantify the error associated with the use of ROM aerodynamics in this type of calculation and is beyond the scope of this paper. However, the authors believe there are two possible sources of the error. The first is in the nonlinearity of the aerodynamics not captured by the dynamically linear ROM, however, in these cases the amplitude of motion is small. The second possible source of error is due to the low order of the aerodynamic model, which keeps only the lowest frequency aerodynamic response. As periodic orbits pass through the switching points of structural stiffness the structural model excites aerodynamic frequencies not necessarily included in the ROM of a particular order. Keeping only the lowest frequency modes has proved adequate for flutter calculations but for the nonsmooth systems considered in this paper, more modes may be required to capture the dynamics very accurately, or the observed behaviour may be a peculiarity of the cases considered.

The second case considers a hysteresis nonlinearity in the flap dof applied to the aerofoil described previously. The parameters of the hysteresis used are defined by

$$
N(\beta) = \begin{cases}
\beta + 0.5 & \text{for} & \beta \langle -0.25 & \text{and} & \dot{\beta}\rangle 0, \\
\beta - 0.5 & \text{for} & \beta \rangle -0.25 & \text{and} & \dot{\beta}\langle 0, \\
0.25 & \text{for} & -0.25 \leqslant \beta \leqslant 0.75 & \text{and} & \dot{\beta}\rangle 0, \\
-0.25 & \text{for} & -0.75 \leqslant \beta \leqslant 0.25 & \text{and} & \dot{\beta}\langle 0, \\
\beta + 0.5 & \text{for} & \beta \rangle -0.75 & \text{and} & \dot{\beta}\rangle 0, \\
\beta + 0.5 & \text{for} & \beta \langle -0.75 & \text{and} & \dot{\beta}\langle 0.
\end{cases}
\tag{28}
$$

The flap LCO bifurcation diagram produced for a Mach number of 0.845 is shown in Fig. 15. This is a relatively simple diagram as there are only period one oscillations which are energetically possible near the flutter boundary for this flow and the particular hysteresis considered. Other demonstrations of the hyperbolic approximation's flexibility can be found in Roberts (2004) where piecewise cubic nonlinearities are also considered.
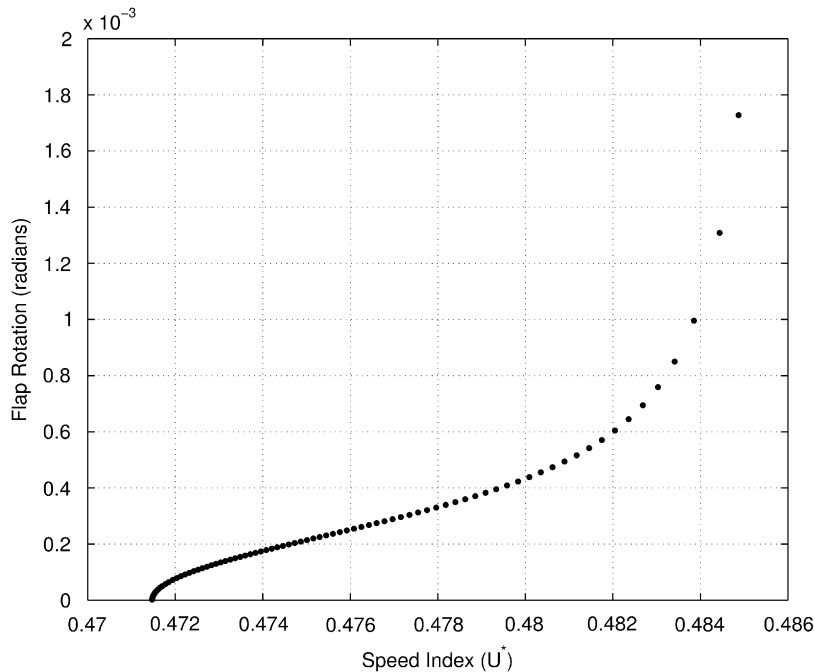
Fig. 15. Flap bifurcation diagram for model with a Hysteresis nonlinearity at Mach 0.845.

5. Conclusions

Methods for the analysis of structurally nonlinear aeroelastic systems in the transonic regime have been demonstrated. The algebraic continuation method allows the accurate capture of the switching points of structural behaviour, but has some drawbacks. The method still requires time simulations to find an initial point on a branch of the bifurcation diagram. A second drawback associated with the current implementation is the definition of branch stability. The second method uses logarithmic and tanh functions to produce accurate approximations to discrete nonlinearities. Coupling these approximations with numerical continuation software is shown to give very accurate results. This method has none of the drawbacks of the algebraic continuation method and the added flexibility of being applicable to general piecewise nonlinear, as well as piecewise linear, systems. Of further interest would be the accuracy of this technique for Grazing bifurcations [see for example Nordmark (1997)]; however, no such bifurcations have been observed in this research.

The transonic results generated show that the methodology employed can generate results rapidly and accurately without the need for costly CFD analysis to be performed. The application of continuation to the problem allows flutter boundaries to be identified rapidly and the effects of nonlinearities on overall system response to be assessed. While attempting to bring such analysis into the computational reach of aircraft design it must also be noted that the nature of aircraft structural nonlinearity is a considerable area of research, which must be complete for these techniques to become of more than academic use. The test cases have also highlighted the need for care in the use of ROMs of transonic aerodynamics; the assumption of the dominance of low frequency response works very well for flutter calculations, but piecewise linear systems may need to retain higher frequency effects.

References

Alighanbari, H., Price, S.J., 1996. The post-Hopf-bifurcation response of an airfoil in incompressible two-dimensional flow. Nonlinear Dynamics 10, 381–400.

Bathe, K.J., 1982. Finite Element Procedure in Engineering Analysis. Prentice-Hall, New Jersey.

Conner, M.D., Virgin, L.N., Dowell, E.H., 1996. Accurate numerical integration of state-space models for aeroelastic systems with freeplay. AIAA Journal 34 (10), 2202–2205.

Dimitriadis, G., Cooper, J.E., 1999. Limit cycle oscillation and suppression. The Aeronautical Journal, 257–263.

Djayapertapa, L., 2001. A computational method for coupled aerodynamic-structural calculations in unsteady transonic flow with active control study. Ph.D. Thesis, University of Bristol.

Doedel, E.J., Champneys, A.R., Fairgrieve, T.F., Kuznetsov, Y.A., Sandstede, B.,Wang, X., 1998. AUTO 97: Continuation and bifurcation software for ordinary differential equations (with HomCont), Concordia University, Montreal, Canada.

Fung, Y.C., 1993. An Introduction to the Theory of Aeroelasticity. Dover, New York.

Gaitonde, A.L., 1994. A dual-time method for the solution of the unsteady Euler equations. The Aeronautical Journal 98 (978), 283–291.

Gaitonde, A.L., Jones, D.P., 2002. Solution of the 2D linearized unsteady Euler equations on moving meshes. In: Proceedings of the Institution of Mechanical Engineers, Part G. Journal of Aerospace Engineering 216 (2), 89–104.

Gaitonde, A.L., Jones, D.P., 2003. Reduced order state-space models from the pulse responses of a linearized CFD scheme. International Journal for Numerical Methods in Fluids 42, 581–606.

Henon, M., 1982. On the numerical calculation of Poincare maps. Physica D 5, 412–414.

Jameson, A.J., Schmidt, W., Turkel, E., 1981. Numerical solutions of the Euler equations by finite volume methods using Runge-Kutta time stepping schemes. AIAA paper 81-1259.

Jones, D.P., Gaitonde, A.L., 2002. System identification and reduction from the pulse responses of a linearised CFD scheme. In: CEAS Aerodynamics Research Conference, Cambridge, UK.

Juang, J.-N., Pappa, R.S., 1985. An eigensystem realization algorithm for modal parameter identification model reduction. Journal Of Guidance, Control and Dynamics 8 (5), 620–627.

Kreiselmaier, E., Lschka, B., 2000. Small disturbance Euler equations: efficient and accurate tool for unsteady load prediction. Journal of Aircraft 37 (5), 770–778.

Kuznetsov, Y.A., 1995. Elements of Applied Bifurcation Theory. Applied Mathematical Sciences 112. Springer, Berlin.

Lee, B.H.K., Gong, L., Wong, Y.S., 1997. Analysis and computation of nonlinear dynamic response of a two-degree-of-freedom system and its application in aeroelasticity. Journal of Fluids and Structures 11, 225–246.

Lee, B.H.K., Price, S.J., Wong, Y.S., 1999. Nonlinear aeroelastic analysis of airfoils: bifurcation and chaos. Progress in Aerospace Sciences 35, 205–334.

Lin, W.B., Cheng, W.H., 1993. Nonlinear flutter of loaded lifting surfaces (I). Journal of the Chinese Society of Mechanical Engineers 14 (5), 446–466.

Liu, L., Wong, Y.S., Lee, B.H.K., 2000. Application of the centre manifold theory in non-linear aeroelasticity. Journal of Sound and Vibration 234 (4), 641–659.

Luber, W.G., 1998. Flutter prediction on a combat aircraft involving backlash on control surfaces. In: Proceedings of the 16th International Modal Analysis Conference, Santa Barbara, CA, pp. 291–299.

Melson, N.D., Sanetric, M.D., Atkins, H.L., 1993. Time accurate Navier–Stokes calculations with multigrid acceleration. NASA CP 3224.

Nordmark, A.B., 1997. Universal limit mapping in grazing bifurcations. Physical Review E 55 (1), 266–270.

Price, S.J., Lee, B.H.K., Alighanbari, H., 1994. Postinstability behaviour of a two-dimensional airfoil with a structural nonlinearity. Journal of Aircraft 31 (6), 1395–1401.

Roberts, I., 2004. Analysis of non-linear aeroelastic systems using numerical continuation. Ph.D. Dissertation, University of Bristol.

Roberts, I., Jones, D.P., Lieven, N.A.J., di Bernardo, M., Champneys, A.R., 2002. Analysis of piecewise linear aeroelastic systems using numerical continuation. In: Proceedings of the Institution of Mechanical Engineers, Part G. Journal of Aerospace Engineering 216 (2), 1–11.

Sedaghat, A., Cooper, J., Wright, J.R., Leung, A.Y.T., 2000. Prediction of nonlinear aeroelastic instabilities. ICAS 2000 Congress, Harrogate, UK, 1–464.

Seydel, R., 1994. Practical Bifurcation and Stability Analysis. From Bifurcation to Chaos. Springer, Berlin.

Schulze, S., 1998. Transonic aeroelastic simulation of a flexible wing. AGARD report 822: 10.1–11.20

Silva, W.A., 1997. Discrete-time linear and nonlinear aerodynamic impulse responses for efficient CFD analyses. Ph.D. Thesis, Department of Applied Science, College of William and Mary, Virginia, USA.

US Department of Defence, 1993. Military specification, Airplane Strength and Rigidity, Vibration, Flutter and Divergence. MIL-A-8870C(AS).

Wong, Y.S., Liu, L., Lee, B.H.K., 2001. Frequency and amplitude prediction of limit cycle oscillations of an airfoil containing concentrated structural nonlinearities. In: 42nd AIAA/ASME/ASCE/AHS/ASC Structures, Structural Dynamics and Materials Conference, AIAA-2001-1293, Seattle.